Preprints (www.preprints.org) | NOT PEER-REVIEWED | Posted: 24 May 2021 doi:10.20944/preprints202105.0544.v1

Fogo volcano (Cape Verde) 2014-2015 eruption: dust characterization and impacts on environment and human health

Carla Candeias[1], Paula F Ávila[2], Célia Alves[3], Carla Gama[3], Cristina Sequeira[1], Eduardo Ferreira da Silva[1], Fernando Rocha[1]

[1]University of Aveiro, Geosciences Department, GeoBioTec, Campus de Santiago, 3810-193 Aveiro, Portugal (candeias@ua.pt).
[2]LNEG National Laboratory of Energy and Geology. Rua da Amieira, Apartado 1089, 4466-901 S. Mamede de Infesta, Portugal.
[3]University of Aveiro, Environment and Planning Department, CESAM, Campus de Santiago, 3810-193 Aveiro, Portugal.

Abstract

Fogo (Fogo island, Cape Verde Republic) is the youngest and most active volcano of the archipelago. The last eruption occurred in 2014–2015. Aiming at studying dust emissions and transport during the eruption period and assessing their impact on air quality and human health, a mineralogical and chemical characterization was undertaken in outdoor dust from all over the island, as well as in the lava resulting from this event. Air quality monitors were used to obtain concentrations of atmospheric particulate matter (PM) and gaseous pollutants. The mineralogical constitution of the samples was analysed by X-ray diffraction and Electron Microprobe, while the chemical characterization was performed through X-ray Fluorescence Spectrometry and ICP-MS. The volcanic rock was found to be tephritic to basanitic, with high potassium content. Several minerals were identified, such as titanian augite with ilmenite, basaltic hornblendes, pyrrhotites, apatites, pyroxenes, basaltic hornblendes and hematites. Concentrations of the particulate matter inhalable fraction (PM_{10}) exceeded the 24-hour mean of 50 µg/m^3 recommended by the World Health Organization. Nevertheless, total volatile organic compounds (TVOCs) showed levels lower than the worrying range. The highest levels of CO_2 were recorded in more populated villages and farthest from the volcano. The Pollution Load Index (PLI) for outdoor dust collected on rooftops was always above 1, suggesting enrichment, with higher values in the dust size fraction < 63 µm. In the same way, the Contamination Factor pointed to high enrichment of As, Ni and Pb, and very high enrichment of Cd in the same size fraction. The Non-carcinogenic Hazard Quotient and Hazard Index estimated for Children suggest that health problems may arise. The Carcinogenic Risk, for all size fractions, was above the target risk. The element that most contributed to the global risk was As, followed by Pb and Co. Ingestion was the main exposure route for all size fractions. The dust size fraction that represented the highest risk was < 63 µm, mostly due to the As concentration.

Keywords: Fogo volcano; volcanic eruption; outdoor dust; PM_{10}; human health Risk

1. Introduction

Volcanic eruptions cause hazardous effects on the environment, climate, exposed population's health, and are also associated with the deterioration of social and economic conditions of surrounding inhabitants [1]. A volcanic eruption is both an international pollutant source and an extended hazard. Natural hazards, such as volcanic eruptions, can be stressful events once are violent natural disasters that impose a threat to human health, as well as to livestock, and can affect global climate [2]. The unfavorable effects of a volcanic eruption depend on the distance, magma viscosity, volcanic ash and gas concentrations. Hazards near volcanic eruptions include toxic volcanic tephra, which can cause problems in the respiratory system, eyes and skin, as well as disposal of materials on soils and water supply contamination [3].

Preprints (www.preprints.org) | NOT PEER-REVIEWED | Posted: 24 May 2021 doi:10.20944/preprints202105.0544.v1

Apart from the immediate life-threatening hazards following a volcano eruption, several other health risks are associated with populations living close to an active volcano [4]. Short-term exposure to volcanic gases can trigger asthma attacks and has been related to respiratory morbidity and mortality and increased irritation of the respiratory tract [5]. Particle deposition in the lung varies with particle diameter [6]. Other possible impacts include ocular and/or skin alterations. Volcanic dust hazards vary with particle mineralogy, chemical concentration, size and morphology. These characteristics depend on the types of eruptions and volcanoes. It is not possible to generalize about the toxicity of volcanic products harmful to humans.

The aims of the present study were to: (a) model mineral dust emissions and transport during the eruption period and their impact on air quality; (b) characterize outdoor dust collected during the 2014-2015 Fogo volcano (Cape Verde) eruption; (c) monitor PM, CO_2, CO and TVOC concentrations during the eruption, and (d) understand the impact of the volcanic products on human health.

2. Materials and methods

Study area: Fogo island (Cape Verde; Fig. 1b) is located in the Atlantic Ocean, 800 km from the northwestern African coast. The Cape Verdean archipelago origin is linked to hotspot magmatism, with melts predominantly alkaline silica-undersaturated of basanitic to tephritic composition, also occurring phonolites and carbonatites [7].

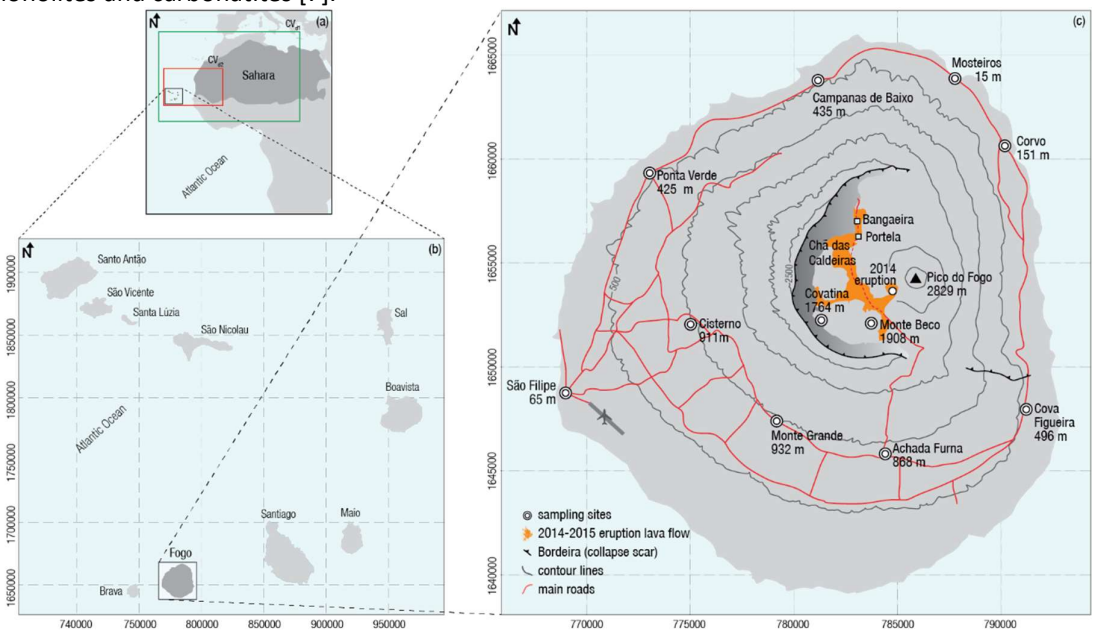

Figure 1. (a) Cape Verde, westwards of African coast, with the CHIMERE simulation domains (CV_{d1} - green and CV_{d2} - red lines; CHIMERE description in section below); (b) Cape Verde archipelago; and (c) Fogo island, 2014 eruption lava and samples sites (adapt. [7]).

Fogo is an active stratovolcano with a maximum altitude at Pico do Fogo (~2,829 m above sea level (asl)). According to Larrue et al. [8], Fogo island is covered by young volcanic rocks of Quaternary age. The collapsed caldera is located in the center of the island [9], with ~8 km in diameter. This collapse gave rise to a caldera scar, locally called Bordeira, with a vertical wall with maximum ~1000 m high and a flat area of ~35 km^2 (~1700 m asl), locally called Chã das Caldeiras, where 2 villages (Bangaeira and Portela) were destroyed during the 2014-2015 eruption (Fig. 1c). This eruption occurred along a SSW-NNE fissure on the eastern flank of Pico Novo (Fig. 2), with the formation of four eruptive craters, emission of gases, pyroclasts and lavas. The eruptive style of the strombolian type began with an explosive phase characterized by the release of gases and pyroclasts, forming an eruptive column with ~6 km high [10]. First lava flows of pahoehoe type changed later to aa lavas. Three eruptive craters with strombolian emissions (gas explosions, pyroclasts and lavas) were formed, with two further lava fronts developed in direction of the destroyed Bangaeira and Portela villages, previously evacuated.

Preprints (www.preprints.org) | NOT PEER-REVIEWED | Posted: 24 May 2021 doi:10.20944/preprints202105.0544.v1

External dust storm events occurred during the 2014 Fogo eruption, causing air quality deterioration. Usually, mineral dust and sea salt are the main contributors to the Cape Verdean aerosol mass [11], with PM exhibiting a strong seasonal trend, with lower values in summer and maximum concentrations in winter due to the outflow of mineral dust from North Africa [12]. Within the framework of CV-DUST (Atmospheric aerosol in Cape Verde region: seasonal evaluation of composition, sources and transport) research project [13], in Praia region (south of Santiago island), it was observed that, in 2011, the daily concentrations exceeded the air quality guidelines proposed by the World Health Organization [14] for $PM_{2.5}$ and PM_{10} in 20 and 30% of the days. Moreover, annual $PM_{2.5}$ and PM_{10} values were also above guidelines.

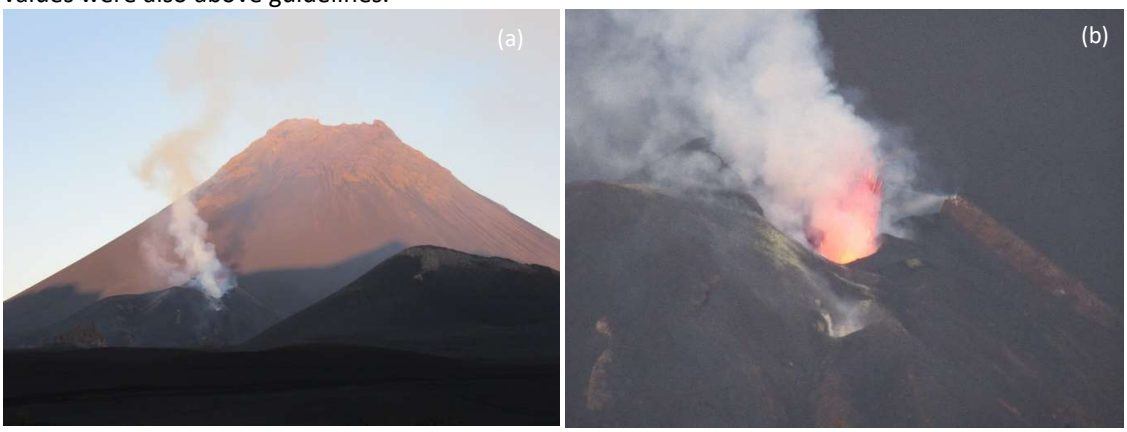

Figure 2. (a) Inactive Pico do Fogo and 2014-2015 eruption location; and (b) detail of the 2014-2015 active craters.

Sampling and air quality monitoring: During the eruption event, for each sampling location (Fig. 1c), outdoor dust samples were collected from the rooftops of private houses using new plastic brooms and shovels. Each sample was georeferenced and preserved in polyethylene bags until laboratory processing. In the laboratory, samples were dried (< 40 ºC), homogenized, sieved (< 2 mm) and partially pulverized to < 170 µm in a mechanical agate mill for chemical analysis. The thoracic fraction of particulate matter (PM_{10}) was collected by low volume sampling (2 L/min) using a Deluxe pump (model 224-PCMTX8) from SKC (Dorset, UK) connected to a size-selective head, also from SKC, equipped with 37 mm quartz filters. The pump was powered by a battery and included a run time programmable unit, a constant pressure controller and a low flow adaptor. Continuous measurements of temperature (T), relative humidity (RH), carbon dioxide (CO_2), carbon monoxide (CO) and total volatile organic compounds (TVOCs) with a 5-min resolution were performed with an IQ-610 Air Quality Probe (Gray Wolf® monitor). A DustTrak DRX 8533 aerosol real time monitor from TSI (also with 5-min resolution) was used for simultaneous monitoring of PM_1, $PM_{2.5}$, PM_4, PM_{10} and total suspended particulate matter (TSP). Additionally, two fresh lava samples were collected in the 2 directions of the lava flow, N and S (Fig. 1c).

During the sampling campaign, informal dialogs were kept with local population, asking about habits and health outcomes before and during the eruption. Respiratory problems, nose and throat irritation with severe coughing and breath difficulty, eye irritation and skin allergies were reported. Also, nervousness and extreme anxiety episodes were communicated by the population as a consequence of the eruption.

Granulometric analysis: Outdoor dust < 2 mm fraction was subject to wet sieving to quantify and analyze separately different size fractions: [-∞, 63[, [125, 63[, [250, 125[, [500, 250[, [500, 1000[and [1000, 2000[µm. The granulometric distribution of the dust fraction < 106 µm was determined at the University of Aveiro, Portugal, using an X-ray grain size analyzer (Micromeritics® SediGraph III Plus). This technique is based on the sedimentation theory (Stokes' law) and the absorption of X-radiation (Beer-Lambert law).

Chemical analysis: Outdoor dust and lava samples were submitted to multielement analysis at the ACME Analytical Laboratories, which is an ISO 9002 Accredited Lab (Vancouver, Canada). A sample of

Preprints (www.preprints.org) | NOT PEER-REVIEWED | Posted: 24 May 2021 doi:10.20944/preprints202105.0544.v1

0.5 g was leached in hot (95 °C) aqua regia (HCl-HNO_3-H_2O), and concentrations were determined by Inductively Coupled Plasma Mass Spectrometry (ICP-MS) for Al, As, Ca, Cd, Co, Cr, Cu, Fe, K, Mg, Mn, Na, Ni, P, Pb, Si, Ti, Zn (detection limits of Cd < 0.1 mg kg^{-1}; Co, Pb < 0.15 mg kg^{-1}; As, Cr, Cu, Ni < 1 mg kg^{-1}; Zn < 1.5 mg kg^{-1}; Mn < 2 mg kg^{-1}; Fe, Mg < 5 mg kg^{-1}; P < 10 mg kg^{-1}; Al, Ca, K, Na, Si, Ti < 20 mg kg^{-1}).

XRD analysis: Mineralogy was determined by powder XRD (LNEG, Portugal) using a Phillips/Panalytical powder diffractometer, model X'Pert-Pro MPD, equipped with an automatic slit. A Cu-X-ray tube was operated at 50 kV and 30 mA. Data were collected from 2 to 70º 2θ with a step size of 1º and a counting interval of 0.02 seconds.

Electron microprobe analysis: The mineralogical characteristics were determined using backscattered electron imaging (BSE) in an electron microprobe JEOL 8500-F (LNEG, Portugal). The operating conditions obtained for the backscattered electron imaging were 15 kV excitation voltage and 30 nA beam current.

Morphology and semi-quantitative chemical analysis: PM_{10} sampled on quartz filters and outdoor dust collected on rooftops were analyzed at UA with a Hitachi S-4100 scanning electron microscope (SEM) coupled to a Bruker Quantax 400 Energy Dispersive Spectrometer (EDS) to assess the morphological, granulometric and semi-quantitative chemical properties of the particles. The identification of inorganic insoluble particles was performed using a mix of protocols for each particle [15].

Precision and accuracy of analyses and digestion procedures were monitored using internal standards, certified reference material and quality control blanks. Results were within the 95% confidence limits. The relative standard deviation was between 5% and 10%.

Modeling mineral dust emissions and transport: The CHIMERE chemistry-transport model [16], forced by 3-D meteorological fields simulated by the WRF model, was used in this study to model the mineral dust cycle over North Africa. This model was previously used over this geographical region with reasonable results since it was able to correctly reproduce the atmospheric dust load and surface concentrations from the daily to the seasonal timescales [17].

The model applied includes only mineral dust and biogenic emissions, i.e., only non-anthropogenic emissions, excluding the volcano. It considers processes that drive the main phases of the dust cycle: saltation and sandblasting for emissions calculations, horizontal advection, and vertical transport, including advection and mixing. Two nested domains were considered (CV_{d1} and CV_{d2}; Fig. 1a) covering the main dust source areas in North Africa, with horizontal resolutions of 0.5° and 0.175°, respectively. Eight vertical layers were used extending from the surface up to 500 hPa. The simulations were performed in time slices of 24 consecutive hours, each new period being initialized by the previous one, being the concentrations continuous in time. Spin-up runs, relative to the 10 days prior to the period of interest, were used to initialize the model. The GOCART global model climatology [18] was used to set the boundary conditions for the larger domain simulation.

Enrichment index (Ei): Ei was calculated by averaging the ratios of elemental concentrations to the lava elemental mean concentration and divided by the number of elements set to assess enrichments in dust samples. An Ei > 1.0 indicates that, on average, the elemental concentration is above the standard level, and that anthropogenic input may have contributed to elemental enrichment [19].

Enrichment Factor (EF): EF is a useful tool to determine the degree of anthropogenic enrichment. EF is calculated by EF = $(element/Fe)_{sample}$ / $(element/Fe)_{lava}$. Iron was selected as reference element for geochemical normalization once its natural concentration tends to be uniform [20]. EF classes are: EF < 1 no enrichment, EF < 3 minor enrichment, 3 < EF < 5 moderate enrichment, 5 < EF < 10 moderately severe enrichment, 10 < EF < 25 severe enrichment, 25 < EF < 50 very severe enrichment, and EF > 50 extremely severe enrichment.

Pollution Factor (CF) and **Contamination Degree (CD)** [21]: CF was calculated for each element (As, Cd, Co, Cr, Cu, Mn, Ni, Pb, Zn) by dividing the mean individual concentration (C_i) by its corresponding baseline value (C_b, estimated from lava samples) to assess external sources. The overall ED for each sample was calculated for each of the nine elements considered: $CD = \left(\sum_{i=1}^{9} CF_i\right)/9$. CF and CD

Preprints (www.preprints.org) | NOT PEER-REVIEWED | Posted: 24 May 2021 doi:10.20944/preprints202105.0544.v1

classifications are: 0 ≤ CF < 1 Low, 1 ≤ CF < 3 Moderate, 3 ≤ CF < 6 High, and 6 ≤ CF Very high Contamination Factor; and 0 ≤ CD < 1.5 None to very low, 1.5 ≤ CD < 2 Low, 2 ≤ CD < 4 Moderate, 4 ≤ CD < 8 High, 8 ≤ CD < 16 Very high, 16 ≤ CD < 32 Extremely high, and 32 ≤ CD Ultra high Contamination Degree.

Pollution Load Index (PLI): PLI provides a simple comparative means to assess the level of enrichment. It was determined as the n^{th} root of the product of the nEF: ELI = $(CF_1 \times CF_2 \times CF_3 \times \cdots \times CFn)^{1/n}$. PLI > 1 suggests environmental deterioration by elemental pollution [22].

Geoaccumulation Index (Igeo): It is defined as Igeo = $Log_2(Cn) / 1.5(Bn)$, where Cn and Bn are the concentrations of each element (n) in dust and lava, respectively. The value of 1.5 is the matrix correction factor due to lithospheric effects [23]. Igeo classes are: Igeo ≤ 0 practically unpolluted, 0 < Igeo < 1 unpolluted to moderately polluted, 1 < Igeo < 2 moderately polluted, 2 < Igeo < 3 moderately to heavily polluted, 3 < Igeo < 4 heavily polluted, 4 < Igeo < 5 heavily to extremely polluted, and 5 > Igeo extremely polluted.

Potential Ecological Risk Index (*PERI*): PERI is defined as the sum of risk factors, defining a potential ecological risk of an element in each sample: $PERI_i = \sum_{i=1}^{7} EF_i = \sum_{i=1}^{7} CF_i \cdot TF$. $PERI_i$ is the Potential Ecological Risk Index for each sample (*i*), EF_i the monomial potential ecological risk factor, CF_i the contamination factor, and *TF* the heavy metal toxic-response factor for each element [21]. Reference values of igneous rock types, soil, freshwater, land plants and land animals were as proposed by Bowen [24]. The PERI classification is as follows: PERI < 150 Low, 150 ≤ PERI < 300 Moderate, 300 ≤ PERI < 600 Considerable, and 600 ≤ PERI Very High Ecological Risk.

Non-carcinogenic and carcinogenic risk assessment: Human health risks were calculated taking into consideration that residents, both children and adults, are directly exposed to dust through three main pathways (a) ingestion, (b) inhalation and (c) dermal absorption. PM_{10} (particles < 10 µm) are more relevant in inhalation processes, nevertheless, coarser sizes are decomposed in the gastrointestinal track. The carcinogenic and non-carcinogenic side effects for each element were computed individually, considering reference toxicity levels for each variable, as extensively described in RAIS [25]. For each selected potentially toxic element (As, Cd, Cr, Co, Cu, Pb, Mn, and Zn) and pathway, the non-cancer toxic risk was estimated by computing the Hazard Quotient (HQ) for systemic toxicity (i.e., non-carcinogenic risk). If HQ > 1, non-carcinogenic effects might occur once exposure concentration exceeds the reference dose (RfD). The cumulative non-carcinogenic hazard index (HI) corresponds to the sum of HQ for each pathway and/or variable. Similarly, HI > 1 indicates that non-carcinogenic effects might occur. Carcinogenic risk, or the probability of an individual to develop any type of cancer over a lifetime as a result of exposure to a potential carcinogen, was estimated by the sum of total cancer risk for the three exposure routes. A risk > 1.00E−06 is classified as the carcinogenic target risk, while values > 1.00E−04 are considered unacceptable [25].

3. Results and discussion

3.1. Modeling mineral dust emissions and transport

Mean PM_{10} surface concentrations within the inner domain (CV_{d2}), between mid-November 2014 and 31 January 2015, are presented in Fig. 3. It is possible to identify two PM_{10} surface concentration hotspots, one in Mauritania, where the highest dust concentrations (> 400 µg/m^3) were simulated. According to the model, Cape Verde PM_{10} mean concentrations were within the range 50–150 µg/m^3.

Preprints (www.preprints.org) | NOT PEER-REVIEWED | Posted: 24 May 2021 doi:10.20944/preprints202105.0544.v1

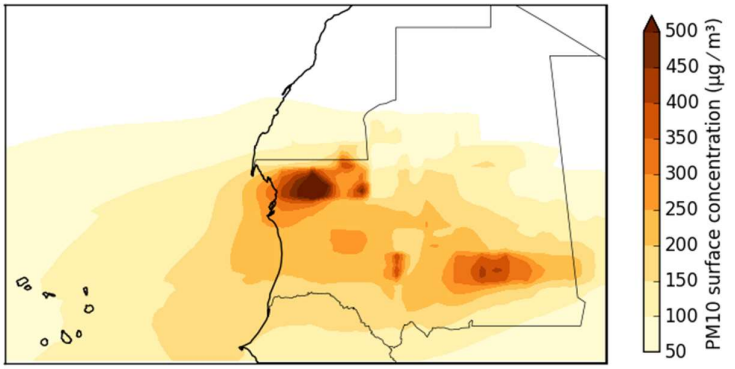

Figure 3. Modeled mean PM_{10} surface concentrations within the inner domain (CV_{d2}) between 15 November 2014 and 31 January 2015.

Desert dust storms impacted the PM levels over the archipelago, starting in December 2014, revealing a remarkable increase of the PM surface level concentrations (Figs. 4, 5). The main dust storm events responsible for the air quality deterioration occurred in December 12 and 20 and January 03, 12 and 28, with PM_{10} modeled concentrations reaching > 400 µg/m^3 daily mean values. These mean concentrations are consistent with the data acquired in S. Filipe (Fig. 1a) by an aerosol monitor, from the National Institute of Meteorology and Geophysics (Cape Verde), on the same period (section 3.4).

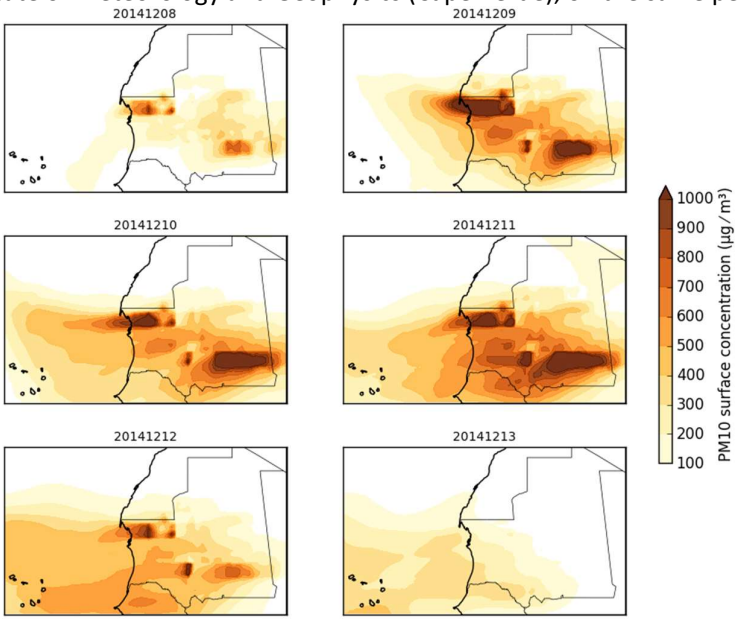

Figure 4. Daily evolution of the modeled mean PM_{10} surface concentrations within the inner domain (CV_{d2}) during a dust storm impacting air quality in Cape Verde (December 08 to 13, 2014).

Preprints (www.preprints.org) | NOT PEER-REVIEWED | Posted: 24 May 2021 doi:10.20944/preprints202105.0544.v1

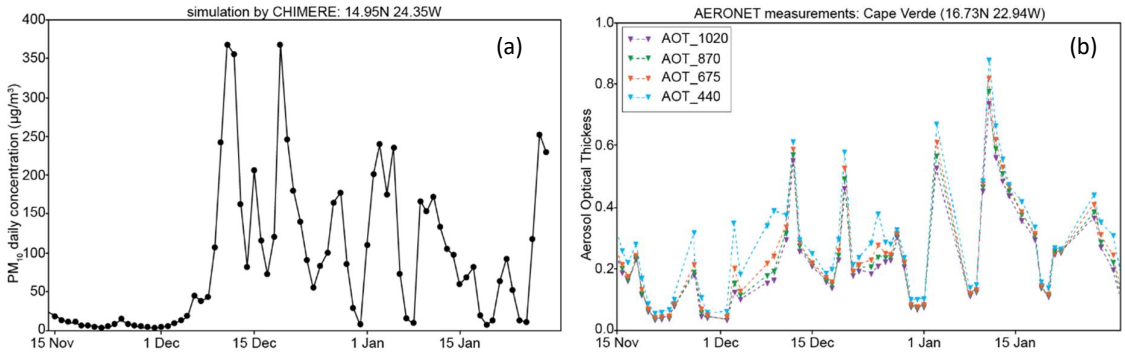

Figure 5. (a) Modeled daily mean PM_{10} concentrations in Fogo Island, Cape Verde, between 15 November 2014 and 31 January 2015 (simulation by CHIMERE: 14.95N 24.35W); and (b) Aerosol optical thickness (Level 2.0; daily averages) observed in the AERONET site installed in Sal Island, Cape Verde, between 15 November 2014 and 31 January 2015.

The model suggests that the source regions that mostly affect the surface Cape Verdean air quality are located over Mauritania (Sahara Desert). In Fig. 4 it is possible to comprehend, with more detail, the evolution of surface concentrations within the inner domain (CV_{d2}), during the first identified dust storm. The emission of dust in the Mauritania hotspots was intensified between December 9 and 11. In this period, dust was transported westwards with maximum surface PM_{10} concentrations being reached around December 12. Aerosol optical thickness (AOD) values (Fig. 5b), registered in the AERONET site of Capo Verde in Sal Island during the same periods, highlight the extent of long-range transport of dust from the African continent.

3.2 PM, CO_2, CO and TVOCs

Regardless sampling location, both PM_{10} and $PM_{2.5}$ concentrations largely exceeded the 24-h daily mean stipulated by the European Air Quality Directive 2008/50/EC and recommended by the World Health Organization [14] of 50 µg/m^3. Highest concentrations were registered in Covatina, directly impacted by one of the two active lava flows. Lowest concentrations, but still above 100 µg/m^3, were measured outside the eruption area, on the north-east to the south-west flanks of the volcano (Ponta Verde, Monte Grande and Cova Figueira). In the three monitoring sites closest to the eruption (Monte Beco, Chã and Covatina), PM_{10} accounted for 65 to 69% of total suspended particulate (TSP). This means that almost 70% of the inhaled particles can pass beyond the larynx and ciliated airways. The percentage of thoracic particles increased to 92 to 96% at other locations, suggesting that small villages and towns within the caldera were strongly impacted by coarse ashes made of tiny fragments of jagged rock, minerals, and volcanic glass, which tend to settle out first. Finer particles remain in the plume and stay airborne while being transported over long distance. The alveolar size fraction encompassed between 51 and 79% of the thoracic particulate mass. The lowest $PM_{2.5}/PM_{10}$ mean ratio was registered in Covatina, near the caldera headwall, whereas the highest value was monitored in Ponta Verde, a settlement in the northwestern part of the island outside the crater rim. All the locations outside the Bordeira scarp presented $PM_1/PM_{2.5}$ ratios in the 0.92–0.94 range. $PM_{2.5}$ comprised higher proportions of ultrafine particles (97–98%) in the vicinities of the volcano.

In São Filipe, the island capital, a Cape Verdean aerosol monitor station (15 min. resolution) was installed between November 28th 2014 and February 15th 2015, the eruption time-lapse. Although some problems with equipment and energy (days 30 November for PM_{10}, 28 November to 6 December for $PM_{2.5}$ and 15 to 19 December for both $PM_{2.5}$ and PM_{10}), data was collected. Figure 6 shows that the mean PM_{10} 24-hour concentration guideline [14] was largely exceeded. Maximum daily mean concentration was registered in December 13th (383 µg/m^3, ranging from 268 to 453 µg/m^3). An extreme concentration range of 479-511 µg/m^3 was recorded between 7:30 pm January 6th and 1:30 am January 7th 2015. WHO [14] also proposed guidelines for $PM_{2.5}$: (a) Interim target-1 (IT-1) of 75 µg/m^3 once values above represent a ~5% increase of short term mortality; (b) IT-2 of 50 µg/m^3 once values above represent a ~2.5% increase of short term mortality; (c) IT-3 of 37.5 µg/m^3 once values above represent a ~1.2% increase of short term mortality; and (d) air quality guideline ($AQG_{PM2.5}$) of 25

Preprints (www.preprints.org) | NOT PEER-REVIEWED | Posted: 24 May 2021 doi:10.20944/preprints202105.0544.v1

µg/m³ (24-h mean). A $PM_{2.5}$ maximum of 107 µg/m³ was measured in January 7th (Fig. 7). The maximum concentration peaked at 123 µg/m³ in January 7th 2015 between 2:30 and 5:50 am. Concentrations of PM_{10} and $PM_{2.5}$ above the guidelines may represent a risk to the human health and are consistent with the volcanic eruption time-lapse and the Sahara Desert dust intrusions (section 3.1).

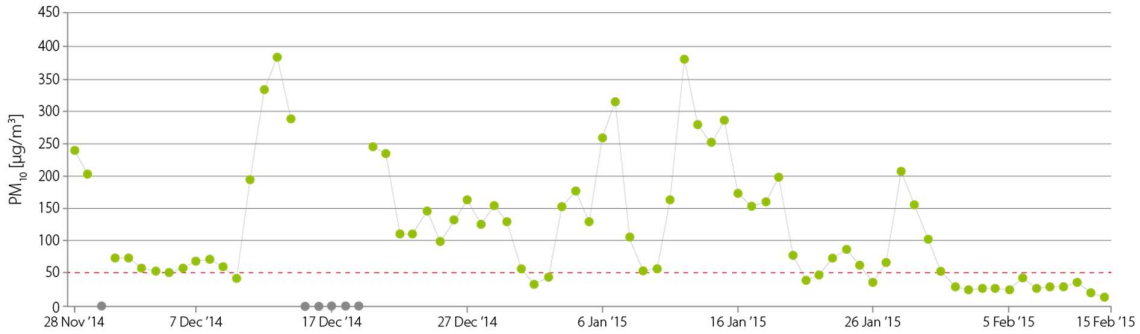

Figure 6. Daily mean PM_{10} concentrations in São Filipe, between November 28th 2014 and February 15th 2015 (courtesy of INMG - National Institute of Meteorology and Geophysics, Cape Verde). The red dashed line represents the daily mean 50 µg/m³ guideline proposed by WHO [14]. Days without readings are in grey dots.

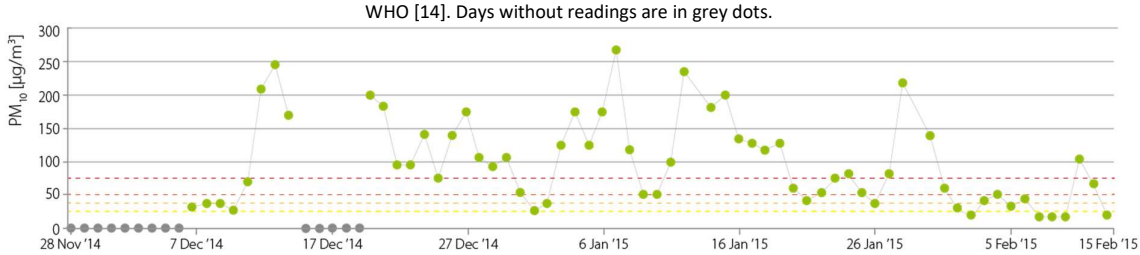

Figure 7. Daily mean $PM_{2.5}$ concentrations in São Filipe of the eruption time-lapse, between December 7th 2014 and February 15th 2015 (courtesy of INMG - National Institute of Meteorology and Geophysics, Cape Verde). Dashed lines represent the daily mean 25 ($AQG_{PM2.5}$), 37.5 (IT-3), 50 (IT-2) and 75 (IT-1) µg/m³ guidelines proposed by WHO [14]. Days without readings are in grey dots.

TVOCs include non-methane hydrocarbons (NMHC) and oxygenated NMHC. Considerable discomfort and headaches are likely if levels fall in the range of 1.2–10 ppm [26]. Only Monte Beco, and sporadically Achada Furna, reached levels close to the lower limit of the worrying range (Fig. 8). There are no enforceable limits for TVOC concentrations, i.e. there is no legal threshold. Much higher VOC concentrations, varying between 2.89 and 35.3 ppm, have been reported by Varshney and Padhy [27] for 13 sites in Delhi, India. However, much lower levels, in the ranges 7–173 ppb and 10–285 ppb in the summer and fall, respectively, have been registered in Los Angeles, California [28]. Concentrations are highly variable, depending on the emission sources, dispersion conditions and atmospheric stability.

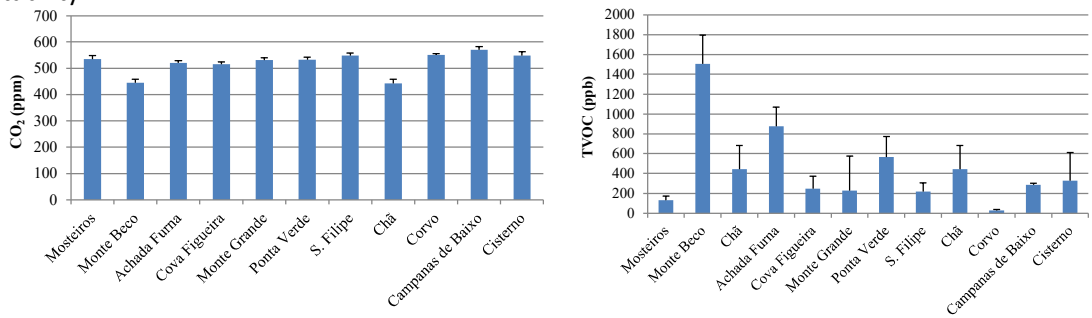

Figure 8. Concentrations of CO_2 and TVOCs in distinct locations of Fogo island.

It has been shown that VOCs from fumaroles mainly consist of C_2–C_5 alkanes and relatively high concentrations of aromatics (benzene and toluene) and C_2–C_3 alkenes (mainly propene and isobutene) [29]. The main mechanism for the production of alkanes is likely related to pyrolysis of organic-matter bearing sediments that interact with the ascending magmatic fluids. Alkanes are then converted to alkene and aromatic compounds via catalytic reactions (dehydrogenation and dehydroaromatisation,

Preprints (www.preprints.org) | NOT PEER-REVIEWED | Posted: 24 May 2021 doi:10.20944/preprints202105.0544.v1

respectively). However, a biogenic origin for the light hydrocarbons cannot be ruled out [30]. It is expected that sulfur and halogen-bearing gaseous compounds, not measured as TVOCs, are dominant in the volcanic plume. Moreover, it should be taken into account that the volcanic plume is ejected at high altitude. Emissions from lava and the fraction of the volcanic plume that reaches the ground suffer dilution by strong winds and changes of their direction. Thus, VOCs may originate, at great extent, from other local sources, other than the volcano. These include natural sources, such as vegetation, and anthropogenic sources, which include emissions from biomass burning, solvent usage and road transport.

The average CO_2 concentrations (Fig. 8) ranged from 445 ppm at Monte Beco (1908 m asl) to 570 ppm at Campanas de Baixo (453 m asl). The highest levels were not registered near the volcano, but rather in more populated villages. CO_2 concentrations around 415 ppm have recently been recorded at the remote observatory near the summit of Mauna Loa, at an altitude of 3400 m asl, which is well situated to measure air masses that are representative of very large areas. CO_2 mixing ratios have been found to be higher in many urban centers worldwide compared to adjacent rural locations, phenomenon known as an "urban CO_2 dome" [31]. These higher mixing ratios are due in part to local traffic emissions. For example, Widory and Javoy [32] measured CO_2 concentrations in air samples collected from various locations in Paris, its suburbs and the surrounding open countryside. These data sets revealed that near-surface atmospheric CO_2 concentrations throughout the country outside Paris averaged 415 ppm, while values in the city sometimes reached as high as 950 ppm.

The CO levels were always close to the detection limit. Due to ejection at high altitude and atmospheric dilution, concentrations of gaseous pollutants seem less affected by the eruption than particles. Ash and gases can be transported either aggregated or separated in the atmosphere. Vertical separation occurs due to the eruption style or by different sedimentation velocity of ash and gases, and horizontal separation due to wind shear [33].

3.3. 2014-15 eruption lava samples

The XRF chemical analysis of lava samples revealed 45 wt% mean SiO_2 content, indicative of basaltic type with high melt temperature (1000–1200 ºC), low viscosity and gas content [34]. Results are consistent with tephra composition (41-45 wt% of SiO_2). According to the total alkali-silica (TAS) diagram [35], this volcanic rock is tephritic to basanitic, with high potassium content. When compared to 1995 Fogo volcano eruption lavas [36], the current samples display relatively higher SiO_2, Al_2O_3 (17.35 wt%), K_2O (3.65 wt%), Na_2O (4.68 wt%), and P_2O_5 (0.93 wt%), similar MnO (0.21 wt%), and lower F_2O_3 (10.85 wt%), MgO (4.32 wt%), and TiO_2 (3.05 wt%) composition.

The backscattered electron imaging of different samples identified several minerals, e.g., matrixes of titanian augite $[(Ca,Na)(Mg,Ti,Fe,Al,)(Si,Al)_2O_6]$ spotted with white ilmenite $[Fe^{2+}TiO_3]$ crystals, vitric materials, basaltic hornblendes $[NaCa_2Fe^{3+}{}_4Ti(Si_6Al_2O_{23})(OH)^2]$, pyrrhotites $[Fe_7S_8]$, apatites $[Ca_5(PO_4)3F]$, pyroxenes (possibly aegirine $[NaFeSi_2O_6]$), basaltic hornblendes $[NaCa_2Fe^{3+}{}_4Ti(Si_6Al_2O_{23})(OH)_2]$ and hematites $[Fe_2O_3]$ (Fig. 9).

Preprints (www.preprints.org) | NOT PEER-REVIEWED | Posted: 24 May 2021 doi:10.20944/preprints202105.0544.v1

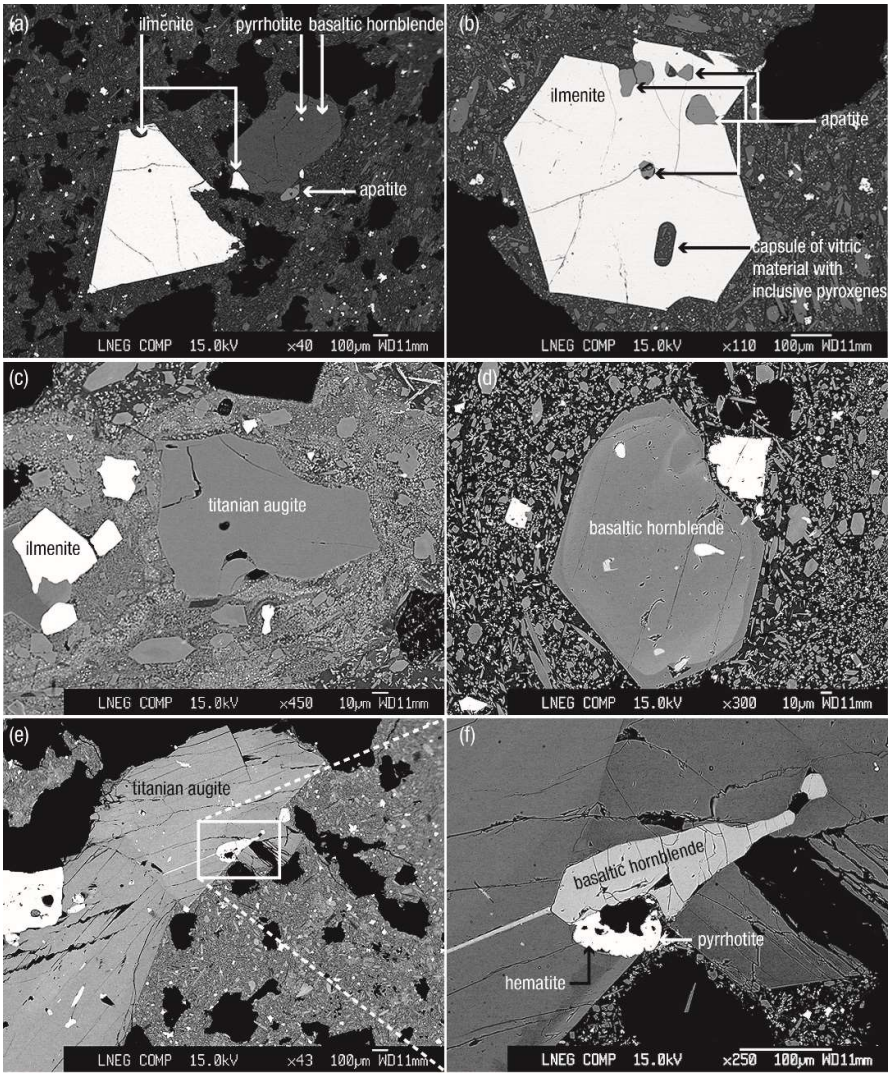

Figure 9. Backscattered electron imaging of Fogo 2014-2015 eruption lava samples.

3.4. Ambient PM_{10} and outdoor dust samples from rooftops

The ICP-MS chemical analysis of outdoor rooftop dust (< 2 mm fraction) and fresh lava samples revealed similar median elemental concentration profiles (Fig. 10). Nevertheless, dust samples from individual locations potentially more impacted by Saharan dust intrusions (NE region) presented higher contents of Fe, Al, Si and Ca than lava. These elements are representative of quartz and other oxides (e.g., FeO_2), carbonates (e.g., $CaCO_3$) and aluminosilicates (e.g., feldspar, clay minerals), characteristic of the Sahara Desert [37]. Minimum and maximum concentrations in dust samples were as follows: Fe [125 000 - 150 000 mg kg^{-1}] > [106 000 - 138 000 mg kg^{-1}] > Al [78 000 - 111 000 mg kg^{-1}] > Ca [86 000 - 100 000 mg kg^{-1}] > Mg [26 000 - 40 000 mg kg^{-1}] > K [21 000 - 28 000 mg kg^{-1}] > Na [24 000 - 32 000 mg kg^{-1}] > Ti [15 000 - 19 000 mg kg^{-1}] > P [4 024 - 4 048 mg kg^{-1}] > Mn [1 691 - 2 178 mg kg^{-1}].

Preprints (www.preprints.org) | NOT PEER-REVIEWED | Posted: 24 May 2021 doi:10.20944/preprints202105.0544.v1

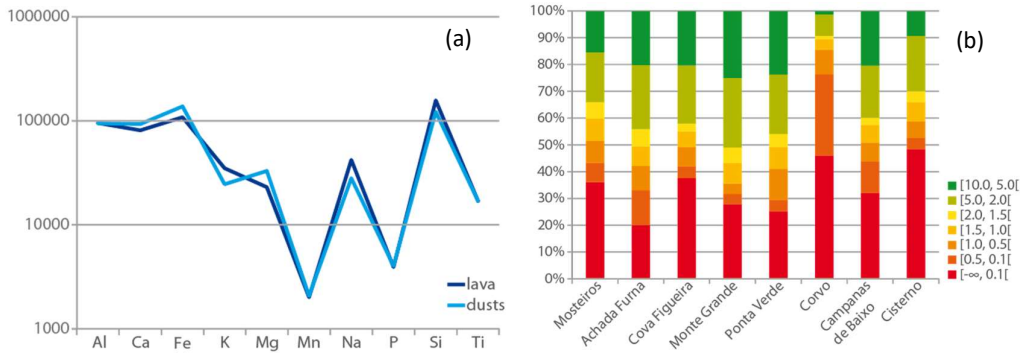

Figure 10. (a) Mean elemental concentration of the 2014-15 lava and outdoor dust samples (< 10 µm); and (b) granulometric relative distribution of outdoor dust.

The Total Granulometric relative Distribution (TRD, <2 mm) of outdoor dust samples suggested a predominance of particles with diameter < 250 µm (~56 %), followed by the size fraction > 125 and < 250 µm (~30 %). In two locations, other fractions prevailed: (a) Corvo, with a dominant fraction in the size range 250 - 500 µm (~55 %); and (b) Cisterno, in the interior of the island, with a prevailing fraction between 63 - 125 µm (~55 %). Among the collected samples, Mosteiros was the village whose dust presented the largest representation of the granulometric fraction < 63 µm (~11%). According to Li et al. [38], the fine fractions (< 150 µm) are the ones that most adhere to human skin, especially children with hand-to-mouth behaviors, being more likely to be ingested and dissolved, accessing the gastric system. Inhalable particles < 10 µm (PM_{10}; Fig. 10) represented 33 to 93 % of the 63 µm fraction, also suggesting an external PM source. PM_{10}-bound constituents and morphology can cause breathing problems and irritation to the respiratory system, while PM_4 can reach deeper regions of the respiratory track. In turn, $PM_{2.5}$ can reach alveoli and induce asthma and even heart attacks, being especially disturbing in children and people with pre-existing health conditions [39]. To humans, fresh volcanic ashes might represent a higher hazard than mineral dust, due to morphology and chemical coatings.

Sharp volcanic minerals were identified in outdoor dust by SEM analysis, together with less sharpen Fe rich particles, with Sahara Desert as possible source (Fig. 11). In Monte Beco several CaF_2 particles were found. The PM_{10} samples collected on quartz filters (Fig. 12) revealed the presence of sea salt [NaCl]. In S. Filipe, the capital of the island and with more traffic, soot particles were also identified. Minerals identified by XRD analysis in lava and outdoor dust samples, in different size fractions, are summarized in Table 1.

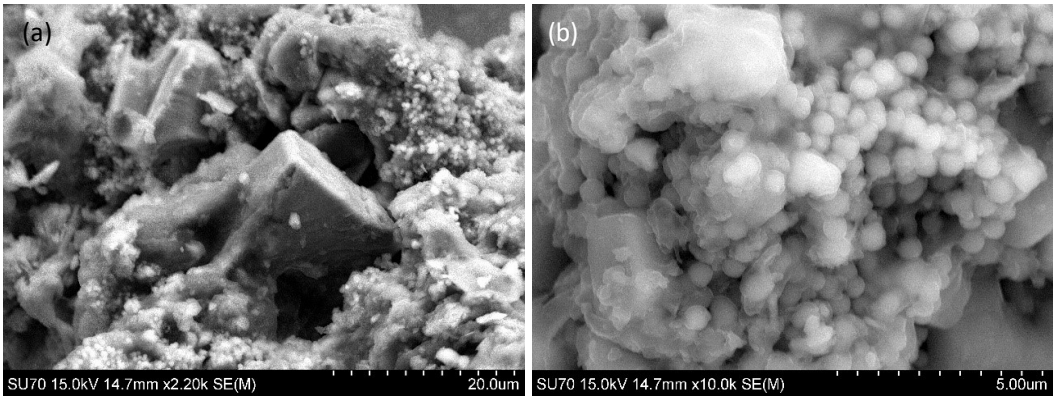

Preprints (www.preprints.org) | NOT PEER-REVIEWED | Posted: 24 May 2021 doi:10.20944/preprints202105.0544.v1

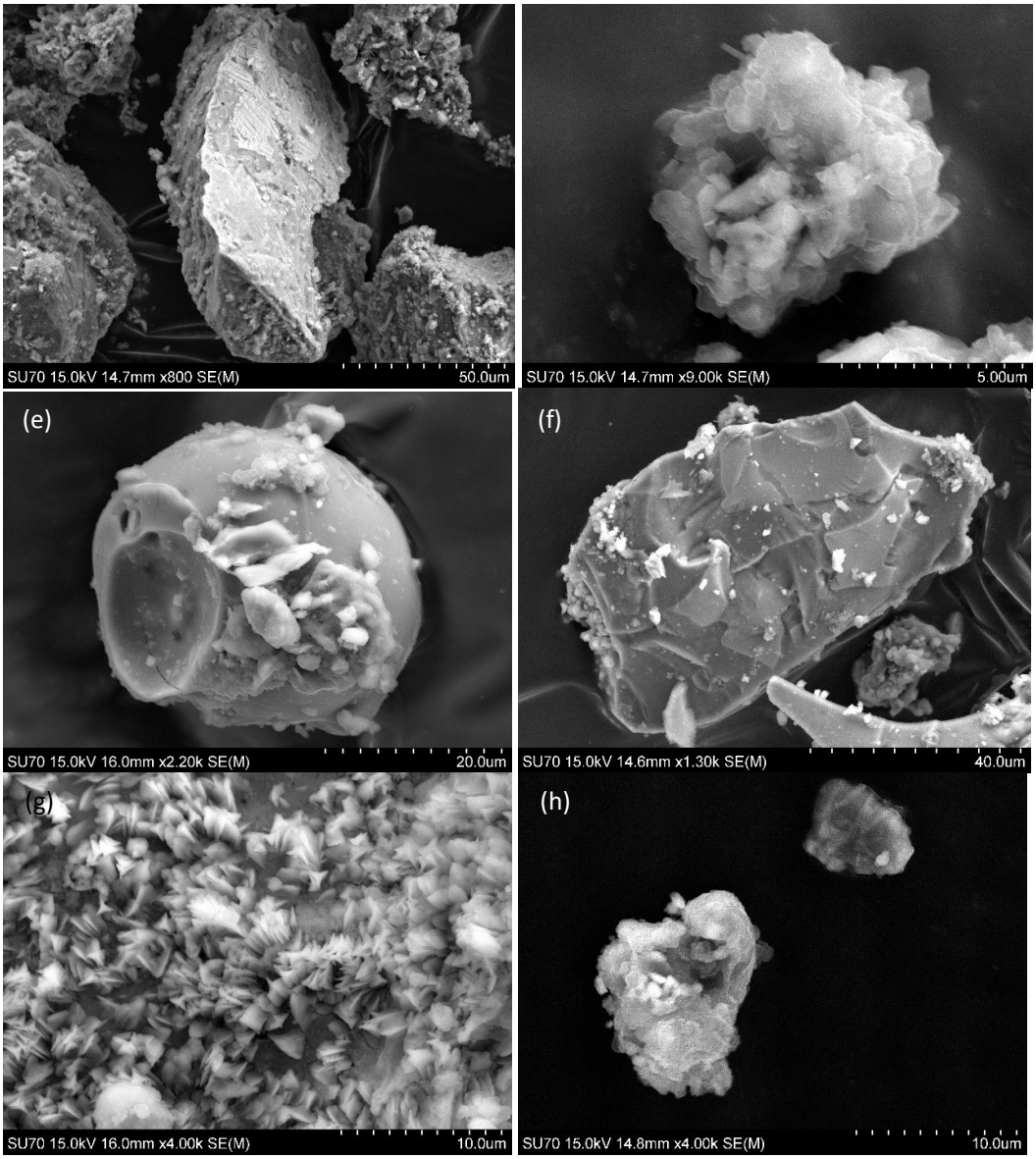

Figure 11. SEM images of dust collected on the rooftops of private houses: (a) Cubic particles of Augite [$(Ca,Na)(Mg,Fe,Al,Ti)(Si,Al)_2O_6$] surrounded by small Fluorite [CaF_2] particles; (b) detail of Fluorite aggregate; (c) Hematite [Fe_2O_3] with marks that suggest brittle fracture processes, covered with Ti oxides cristals; (d) particle aggregate with quartz and Haüyne [$(Na,Ca)_{4\text{-}8}Al_6Si_6(O,S)_{24}(SO_4,Cl)_{1\text{-}2}$]; (e) Fe oxide with vesicular marks; (f) sharp Fe and Ti rich particle with marks resulting from brittle fracture conditions; (g) raft-like calcite aggregate; (h) rounded Fe and Ca rich particles (Sahara dusts?).

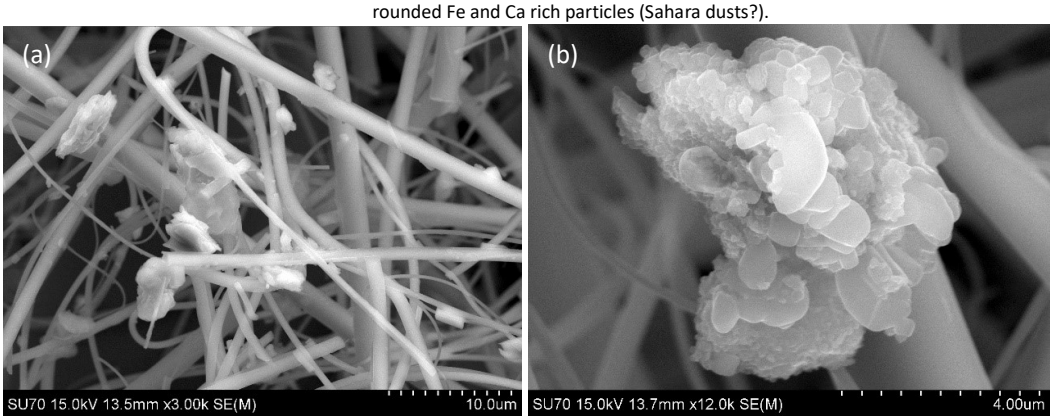

Preprints (www.preprints.org) | NOT PEER-REVIEWED | Posted: 24 May 2021 doi:10.20944/preprints202105.0544.v1

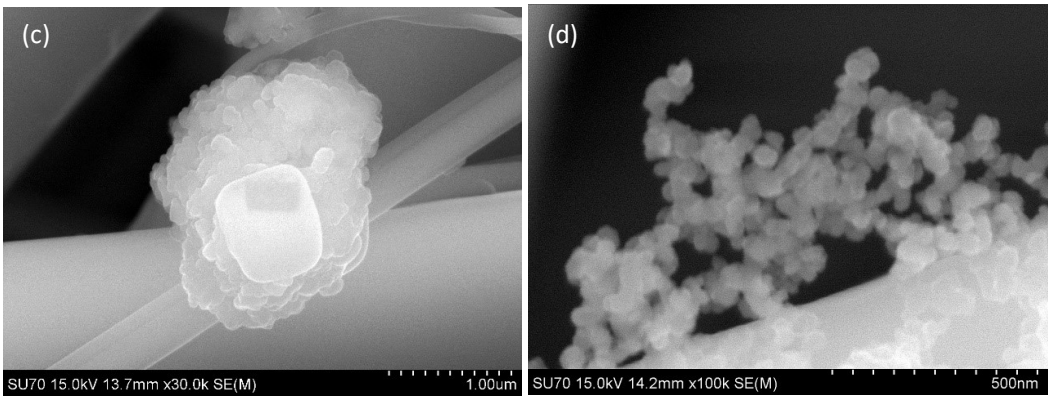

Figure 12. SEM images of PM_{10} collected on quartz filters: (a) PM_{10} enriched in Fe, S and Ti; (b) Ca and S rich particles agglomerate (Bassanites?) with inhalable size; (c) salt [NaCl] on top of a Si, Fe, Ti enriched particle; (d) soot.

Table 1. Main mineral occurrence (DRX analysis) on the two lavas and different dust size fractions [µm].

Mineral	Lava	Outdoor dust					
		[1000, 2000[	[500, 1000[	[500, 250[	[250, 125[	[125, 63[	[-∞, 63[
Aegirine $[(Na,Ca)(Fe^{3+},Fe^{2+},Mg,Al)Si_2O_6]$	++	++++	++++++	+++++	++		
Augite $[(Ca,Na)(Mg,Fe,Al,Ti)_2(Si,Al)_2O_6]$	++	+++++++	+++++++	+++++++	+++++++	+++++++ +	++++
Calcite $[CaCO_3]$			+++	++	+	++	++++
Diopside $[CaMgSi_2O_6]$	++	+++++	+++++	+++++++ +	+++++++ +	+++++++ +	++++++ +
Fluorite $[CaF_2]$	+	+++++	+++	+++	+++	+	++
Forsterite $[Mg_2SiO_4]$		+++	+++	++	++	++	++
Hematite $[Fe_2O_3]$	++	++	++	+++++	+++	++	+++
Ilmenite $[Fe^{2+}TiO_3]$	++	+	+++	++++++	+++++	+++	+++
Leucite $[KAlSi_2O_6]$	++	+++++	++++++	+++++			
Magnesioferrite $[MgFe^{3+}O_4]$	++			++	++++	+++++	++++

Fogo island inhabitants, particularly those living in Chã das Caldeiras, are exposed to air deterioration, especially during eruptions and Sahara dust intrusions. Eyes and respiratory tract irritation were reported, not only during the 2014-2015 volcanic eruption, but also previously. Dental and bone problems on the interviewed inhabitants were described, conceivably related to F^- inhalation (dusts and gases) and ingestion (hand-to-mouth, food and drinking water). Association between fluorides geochemistry and health is well studied [e.g., 40, 41, 42]. Fluoride metabolism varies with solubility, structure, reactivity, and release of F^- ions. In humans, the main F^- absorption path is the gastrointestinal tract, by inhalation and ingestion (drinking and diet), with 80–90% of consumed F^- absorbed within 30 minutes [43]. Nevertheless, the F^- content varies with individual uptake and excretion. Usually, 45–60% of the ingested F^- is excreted in urine, with the rest recirculated into the plasma or deposited into the bones [44]. The island population is strongly dependent on agriculture, livestock and groundwater. Waters for drinking and cooking are obtained by rainwater harvesting, dug wells and deep bore holes. Agriculture products and livestock are exported to other islands of the archipelago. The volcanic expelled products contribute to inhalation and ingestion of dust and gases in excess, but also through consumption of food and water enriched in potentially toxic elements.

3.5. Ecological and human health impact

For the calculation of different indexes, mean concentrations of lava samples were used as background values, to understand the external sources of dust enrichment. Two sets of variables were studied: (a)

Preprints (www.preprints.org) | NOT PEER-REVIEWED | Posted: 24 May 2021 doi:10.20944/preprints202105.0544.v1

major elements - Al, Ca, Fe, K, Mg, Si, and Ti; and (b) elements potentially linked to anthropogenic sources - As, Cd, Co, Cr, Cu, Mn, Ni, Pb, and Zn. Three size fractions were selected (< 63, 63-125 and 125-250 µm), once particles with diameter < 250 µm are considered to adhere to hands and may be ingested by hand-to-mouth behaviors [45].

The group of major elements, linked to the Fogo volcano geochemical composition, suggests a small contribution from external sources. The Enrichment Index (Ei; Table 2) was slightly over 1, with a maximum of 1.5 for the dust fraction sized 125 - 250 µm of Ponta Verde. These results are confirmed by the Contamination Degree (CD), Pollution Load Index (PLI) and Potential Ecological Risk Index (PERI), which enabled to classify all locations with a low-grade enrichment, although Ponta Verde presented higher results. The Geoccumulation Index (Igeo), Enrichment Factor (EF) and Contamination Factor (CF) also showed a low external contribution in all samples and fractions, with slightly higher Mg concentrations that in lava samples.

Table 2. Enrichment index (Ei), Geoaccumulation Index (Igeo), Enrichment Factor (EF), Contamination Factor (CF), Contamination Degree (CD), Pollution Load Index (PLI) and Potential Ecological Risk Index (PERI) for Al, Ca, Fe, K, Mg, Si, and Ti in outdoor dust samples sized < 63, 63-125 and 125-250 µm.

	< 63 µm			**63 - 125 µm**			**125 - 250 µm**		
	mean	**min**	**max**	**mean**	**min**	**max**	**mean**	**min**	**max**
Ei	1.0	1.0	1.1	1.2	1.1	1.3	1.2	1.0	1.5
$Igeo_{Al}$	-0.4	-0.6	-0.2	-0.7	-1.1	-0.5	-0.7	-1.2	-0.5
$Igeo_{Ca}$	-0.3	-0.3	-0.2	-0.1	-0.3	0.1	-0.2	-0.3	0.0
$Igeo_{Fe}$	-0.2	-0.3	-0.1	0.0	-0.2	0.1	0.0	-0.3	0.4
$Igeo_{K}$	-0.8	-0.9	-0.6	-0.8	-1.7	-0.4	-1.2	-2.6	-0.5
$Igeo_{Mg}$	-0.1	-0.3	0.1	0.3	0.2	0.7	0.4	-0.5	0.9
$Igeo_{Si}$	-0.7	-0.8	-0.5	-0.5	-0.6	-0.3	-0.5	-0.8	-0.3
$Igeo_{Ti}$	-0.4	-0.5	-0.3	-0.2	-0.3	-0.1	-0.1	-0.3	0.3
EF_{Al}	0.8	0.7	0.8	0.5	0.3	0.7	0.5	0.2	0.8
EF_{Ca}	0.9	0.9	0.9	0.8	0.8	1.2	0.8	0.5	1.0
EF_{Fe}	1.0	1.0	1.0	1.0	1.0	1.0	1.0	1.0	1.0
EF_{K}	0.5	0.5	0.6	0.4	0.2	0.8	0.4	0.0	0.7
EF_{Mg}	1.1	1.0	1.3	1.7	1.2	1.9	1.7	0.8	2.5
EF_{Si}	0.6	0.5	0.8	0.6	0.5	0.8	0.6	0.3	1.0
EF_{Ti}	0.8	0.6	1.0	0.9	0.7	1.0	0.9	0.7	1.1
CF_{Al}	1.0	0.8	1.2	0.8	0.3	1.0	0.7	0.5	0.9
CF_{Ca}	1.1	1.1	1.7	1.3	1.1	1.6	1.2	1.1	1.5
CF_{Fe}	1.3	1.2	1.4	1.4	1.3	1.7	1.5	1.2	2.3
CF_{K}	0.7	0.6	0.8	0.7	1.8	3.7	0.5	0.1	0.9
CF_{Mg}	1.4	1.1	1.7	2.1	1.8	3.1	2.5	0.9	3.7
CF_{Si}	0.8	0.7	0.9	0.9	0.7	1.1	0.9	0.7	1.1
CF_{Ti}	1.0	0.9	1.1	1.2	1.1	1.4	1.3	1.1	2.0
CD	1.0	1.0	1.1	1.2	1.1	1.3	1.2	1.0	1.5
PLI	1.0	0.9	1.1	1.1	1.0	1.2	1.1	0.9	1.1
PERI	28	27	29	32	30	34	34	30	44

The Enrichment index for a set of elements with a potential link to anthropogenic sources (Table 3) suggest the contribution of an external source to the dust samples, irrespective of the size fractions.

Preprints (www.preprints.org) | NOT PEER-REVIEWED | Posted: 24 May 2021 doi:10.20944/preprints202105.0544.v1

The minimum values were found to be higher in the size fraction < 63 µm, especially in samples from the NE sector of the island. Nevertheless, the maximum Ei values (4.9 in 125 – 250 µm and 4.2 in 63 – 125 µm) were observed in coarser fractions from Ponta Verde, a village not directly impacted by volcanic emissions. The Geoaccumulation index indicates a small external contribution for all size fractions and elements. The highest Igeo values (2.4 Cr and 2.5 Cu in dust sized 125-250 µm, and 2.0 Cr and 2.4 Cu in the 63-125 µm size fraction) were obtained in dust from Ponta Verde, classified as moderately to heavily contaminated. In the same location, As presented a maximum Igeo value of 1.5, in the size fraction < 63 µm, classified as moderately contaminated. The EF also suggested a moderate enrichment in this size fraction, presenting its maximum value in Ponta Verde (EF = 3.4). Higher Ni EF values, classified with moderately severe enrichment, were found in size fractions 63 - 125 and 125 - 250 µm, in Mosteiros, Campanas de Baixo and Ponta Verde villages, located in the N of the island, the area most affected by external NE-SW dust contribution. Also, Cr presented EF > 5 in Ponta Verde for the same size fractions. The same results were obtained with the Contamination Factor. CF also displayed a high contamination of As, Ni and Pb, and very high contamination of Cd in the size fraction < 63 µm of dust from Ponta Verde and Cisterno villages. Nevertheless, the Contamination Degree presented its maximum in the 125 - 250 µm size fraction of dust from Ponta Verde (CD = 4.6, high contamination). Other size fractions of this location were classified with moderate contamination. Also, coarser dust fractions from Cova Figueira, Campanas de Baixo and Achada Furna were classified as having a moderate CD.

The Pollution Load Index presented values above 1 in all samples, except for the 125 - 250 µm size fraction of dust from Cisterno, suggesting an external contribution for the selected elements. Higher PLI values were found in the size fraction < 63 µm, especially in Ponta Verde and Campanas de Baixo villages. The same results were obtained with the Potential Ecological Risk Index. All the samples sized < 63 µm were classified of extreme risk (PERI mean value of 431). The 125 - 250 µm size fraction of dust from Monte Grande presented the lowest PERI value (144), while the highest PERIs were obtained in Ponta Verde, Mosteiros and Campanas de Baixo (551, 491, and 334, respectively). For the size fraction 63 - 125 µm, the highest PERI values were found in Mosteiros (502) and Ponta Verde (492), whose samples were categorized of severe risk, whereas other samples were classified with moderate risk.

Table 3. Enrichment index (Ei), Geoaccumulation Index (Igeo), Enrichment Factor (EF), Contamination Factor (CF), Contamination Degree (CD), Pollution Load Index (PLI) and Potential Ecological Risk Index (PERI) for As, Cd, Co, Cr, Cu, Mn, Ni, Pb, and Zn in outdoor dust samples, fractions < 63, 63-125 and 125-250 µm.

	Ø < 63 µm			Ø 63 - 125 µm			Ø 125 - 250 µm		
	mean	min	max	mean	min	max	mean	min	max
Ei	2.5	2.2	2.6	2.1	1.2	4.2	2.4	1.1	4.9
$Igeo_{As}$	1.1	0.6	1.5	-0.3	-0.4	0.8	-0.3	-0.4	0.6
$Igeo_{Cd}$	0.9	0.3	1.4	0.0	-0.5	1.3	-0.3	-0.8	0.0
$Igeo_{Co}$	-0.1	-0.1	-0.1	0.0	-0.2	0.5	0.2	-0.2	0.9
$Igeo_{Cr}$	0.3	0.3	0.4	0.3	-0.9	2.0	0.5	-2.0	2.4
$Igeo_{Cu}$	0.4	0.4	0.5	0.3	0.1	0.7	0.0	-0.2	0.2
$Igeo_{Mn}$	-0.4	-0.4	-0.3	-0.3	-0.4	-0.3	-0.4	-0.5	-0.3
$Igeo_{Ni}$	0.8	0.8	0.8	0.9	0.3	2.4	1.3	0.1	2.5
$Igeo_{Pb}$	0.6	0.4	0.8	-0.1	-0.5	1.1	-0.6	-1.3	0.2
$Igeo_{Zn}$	-0.1	-0.2	0.1	-0.1	-0.4	0.5	-0.2	-0.4	0.2
EF_{As}	3.1	2.9	3.4	0.8	0.6	2.6	0.8	0.4	1.6
EF_{Cd}	3.2	1.8	4.5	0.8	0.6	4.3	0.8	0.3	1.1
EF_{Co}	1.1	1.0	1.2	1.3	0.9	1.5	1.3	1.0	1.6
EF_{Cr}	1.7	1.4	1.9	3.0	0.5	6.6	3.0	0.2	6.8
EF_{Cu}	1.8	1.8	1.9	1.1	1.2	2.3	1.1	0.5	1.5
EF_{Mn}	0.8	0.8	0.8	0.7	0.6	0.8	0.7	0.5	0.8

Preprints (www.preprints.org) | NOT PEER-REVIEWED | Posted: 24 May 2021 doi:10.20944/preprints202105.0544.v1

EF_{Ni}	2.6	2.3	3.0	4.4	1.5	9.6	4.4	1.3	8.0
EF_{Pb}	2.2	1.6	2.7	0.6	0.6	3.5	0.6	0.2	1.0
EF_{Zn}	1.2	0.9	1.5	0.9	0.7	1.9	0.9	0.8	1.1
CF_{As}	3.9	3.9	3.9	1.3	1.0	3.4	1.2	1.0	2.7
CF_{Cd}	4.2	2.1	6.3	1.8	0.9	5.7	1.1	0.7	1.5
CF_{Co}	1.4	1.4	1.4	1.6	1.3	2.5	1.9	1.2	3.8
CF_{Cr}	2.1	2.0	2.2	3.0	0.6	11.1	**5.1**	0.2	15.9
CF_{Cu}	2.3	2.2	2.5	2.1	1.7	3.1	1.6	1.2	1.9
CF_{Mn}	1.0	1.0	1.1	1.1	1.0	1.2	1.0	0.9	1.1
CF_{Ni}	3.3	3.3	3.4	5.0	2.0	15.9	**7.2**	1.6	17.8
CF_{Pb}	2.7	2.2	3.2	1.7	0.9	4.6	0.9	0.4	1.8
CF_{Zn}	1.4	1.2	1.7	1.5	1.0	2.5	1.2	1.0	1.8
CD	2.0	1.8	2.3	1.7	1.0	3.9	2.1	0.9	4.6
PLI	2.2	2.2	2.3	1.7	1.1	2.8	1.6	1.0	2.3
PERI	431	414	448	273	158	506	292	144	551

For children, the Non-carcinogenic Hazard Quotient (Table 4) through Ingestion ($HQ_{ChildIng}$) and the Hazard Index ($HI_{ChildTotal}$) were above the threshold of 1 (mean HQ = HI = 1.4 in all samples and size fractions), suggesting that non-carcinogenic health outcomes might occur once exposure to elements is higher than the reference dose. The highest HQ (1.6) and HI (1.7) were found in the fraction 63 - 125 µm of dust collected in S. Filipe, the island Capital, for which Co, Cu and Mn concentrations were the main contributors, representing 24.4, 3.3, and 71.3 %, respectively, of the Hazard. In all samples and fractions, Mn accounted for 71.3 to 83.9 % of the total HI.

The Carcinogenic Risk (Table 4) of all size fractions was above the target value of 1.00E−6. However, regardless of the samples, the risk was always < 1.00E−4. Arsenic was the element that most contributed to the risk, accounting for 86.2 to 95.8 % of the total, followed by Pb (1.7 to 9.7 %) and Co (1.1 to 10.6 %). Ingestion was found to be the main exposure route for all dust size fractions, representing 78.5 to 87.3 % of the total risk posed by the three exposure routes. The finest size fraction (< 63 µm) was the one with the highest risk, mostly due to As, whose concentrations accounted for 91.4 to 95.5 % of the total. The lowest total risk value was found in Monte Grande, located in the interior of the island, for the 125 – 250 µm size fraction, while the highest was observed in the < 63 µm fraction of Ponta Verde.

Table 4. Non-carcinogenic Hazard and Carcinogenic Risk posed by outdoor dust samples, in fractions < 63, 63-125 and 125-250 µm.

Dust Fractions		**$HQ_{ChildIng}$**	**$HI_{ChildTotal}$**	**$Risk_{AsIng}$**	**$Risk_{AsTotal}$**	**$Risk_{TotalIng}$**	**$Risk_{Total}$**
< 63 µm	mean	1.4	1.4	6.34E-06	7.24E-06	6.63E-06	7.61E-06
	min	1.3	1.3	6.34E-06	7.24E-06	6.58E-06	7.56E-06
	max	1.5	1.5	6.34E-06	7.24E-06	6.67E-06	7.65E-06
63 - 125 µm	mean	1.4	1.4	2.11E-06	2.41E-06	2.29E-06	2.68E-06
	min	1.3	1.3	1.62E-06	1.85E-06	1.72E-06	2.02E-06
	max	1.6	1.7	5.57E-06	6.35E-06	6.04E-06	6.92E-06
125 - 250 µm	mean	1.4	1.4	1.97E-06	2.25E-06	2.05E-06	2.45E-06
	min	1.2	1.3	1.62E-06	1.85E-06	1.65E-06	2.00E-06
	max	1.5	1.5	4.40E-06	5.02E-06	4.58E-06	5.34E-06

$HQ_{ChilIng}$ - Non-carcinogenic Hazard Quotient for children by ingestion; $HI_{ChildTotal}$ - Cumulative non-carcinogenic Hazard Index of all elements and routes; $Risk_{AsIng}$ - Carcinogenic Risk posed by As Ingestion; $Risk_{TotalIng}$ - Risk by Ingestion for total elements; $Risk_{Total}$ - Total Risk posed by all elements and exposure routes.

 doi:10.20944/preprints202105.0544.v1

4. Conclusions

Modeling of long-range transport of mineral dust between mid-November 2014 and January 2015 pointed out Mauritania (Sahara Desert) as the main external dust mineral source affecting the Cape Verdean air quality, highlighting the intrusion of dust from continental Africa. PM_{10} and $PM_{2.5}$ concentrations largely exceeded the guidelines suggested by the World Health Organization, in line with the volcanic eruption time-lapse and the Sahara Desert dust outbreaks. The levels of Total Volatile Organic Compounds (TVOCs) were below the worrying range. The highest levels of CO_2 were recorded in more populated villages and not next to the volcanic eruption craters. The chemical analysis of lava samples revealed a SiO_2 content indicative of basaltic type with high melt temperature, low viscosity and gas content. This volcanic rock is tephritic to basanitic, with high potassium content. Several minerals were identified, such as titanian augite with ilmenite, basaltic hornblendes, pyrrhotites, apatites, pyroxenes, basaltic hornblendes and hematites.

Outdoor dust and fresh lava samples revealed similar median elemental concentrations, with high contents of Fe, Al, Si and Ca. The granulometric distribution of outdoor dust was dominated by particles with diameter < 250 µm, followed by the size fractions > 125 and < 250 µm. The finest particle sizes (< 250 µm) are the ones that most adhere to human skin. The PM_{10} inhalable fraction represented the highest percentage of the dust sizes < 63 µm, factor that can potentiate breathing problems and irritation to the respiratory tract. Fogo inhabitants exposed to air deterioration reported irritation of the respiratory tract and eyes. Dental and bone problems were also described, possibly related to inhalation of F^-, present either in dust or in gaseous form, and ingestion (hand-to-mouth, food and drinking water). The island population is strongly dependent on agriculture, livestock and groundwater. The volcanic expelled products likely contributed to inhalation and ingestion of dust and gaseous pollutants in excess, but also through consumption of food and water enriched in potentially toxic elements.

According to the Enrichment Index (Ei), Contamination Degree (CD), Pollution Load Index (PLI) and Potential Ecological Risk Index (PERI), calculated based on the content of Al, Ca, Fe, K, Mg, Si, and Ti, all locations were classified with a low-grade enrichment. The Geoccumulation Index (Igeo), Enrichment Factor (EF) and Contamination Factor (CF) showed a low external contribution to all samples and size fractions. The Enrichment Index for elements with a potential link to anthropogenic sources (As, Cd, Co, Cr, Cu, Mn, Ni, Pb, and Zn) suggested the input of external sources to all size fractions. The Geoaccumulation Index pointed out a small external contribution to all size fractions and elements, with values indicating that dust samples were moderately to heavily enriched by these metal(loid)s. In addition, the Enrichment Factor suggested a moderate enrichment in the size fraction < 63 µm. The same results were obtained with the Contamination Factor, which pointed out to high contamination of As, Ni and Pb, and very high contamination of Cd. The Pollution Load Index presented values above 1 in all samples, categorizing dust as polluted. Higher PLI values were found in the size fraction < 63 µm. The Potential Ecological Risk Index also enabled to include all samples < 63 µm in the "extreme risk" group.

The Non-carcinogenic Hazard Quotient and the Hazard Index from the exposure of children to elements through ingestion were above 1, suggesting that non-carcinogenic health outcomes might occur, since concentrations were higher than the reference doses. The Carcinogenic Risk associated with all dust size fractions was above the target risk of 1.00E-06. Arsenic was the element that most contributed to the global risk, followed by Pb and Co. Ingestion was found to be the main exposure route of dust-bound metals in all size-segregated fractions. The size fraction < 63 µm was the one representing a higher risk, mostly due to the concentration of As.

It is known that the total concentration of potentially toxic elements can overestimate the risk for humans. To understand the bioaccessible fraction (BAF) in lungs, gastric and gastrointestinal phases of the outdoor dust, the Artificial Lysosomal Fluid (ALF) and Unified Bioaccessibility Method (UBM) assays are being done. Also, the edible plants most consumed in the island are being analyzed and BAF being estimated.

Authorship contribution statement: Carla Candeias: sampling, conceptualization, funding, methodology, formal analysis, supervision, writing – original draft. Paula Ávila: methodology, formal analysis, writing – review and editing. Célia Alves: methodology, formal analysis, writing – review and editing. Carla Gama: methodology, formal analysis, writing – review and editing. Eduardo Ferreira da Silva: writing – review and editing. Fernando Rocha: funding, writing – review and editing.

Declaration of interest: The authors declare no known competing financial interests or personal relationships that could have appeared to influence the work reported in this paper.

Acknowledgments: The sampling campaign was supported by the Portuguese Foundation for Science and Technology (FCT), with an emergency financial support provided to C4G (Collaboratory for Geosciences) during the 2014-2015 Fogo volcano eruption monitoring mission. Carla Candeias grant SFRH/BPD/99636/2014, respectively, from FCT. We are also grateful for the support to GeoBioTec (UID/GEO/04035/2019 + UIDB/04035/2020) and CESAM (UIDB/50017/2020 + UIDP/50017/2020) to FCT/MCTES through national funds, and co-funding by FEDER, within the PT2020 Partnership Agreement and Compete 2020.

References

1. Barone, G.; De Giudici, G.; Gimeno, D.; Lanzafame, G.; Podda, F.; Cannas, C.; Giuffrida, A.; Barchitta, M.; Agodi, A.; Mazzoleni, P. Surface reactivity of Etna volcanic ash and evaluation of health risks. Sci Total Environ **2021**, 761, 143248, doi 10.1016/j.scitotenv.2020.143248
2. Stenchikov, G. The role of volcanic activity in climate and global changes (Chapter 29). Eds: T.M. Letcher. Climate Change (3rd Ed), Elsevier **2021**, 607-643, doi 10.1016/B978-0-12-821575-3.00029-3
3. Tomašek, I.; Damby, D.E.; Stewart, C.; Horwell, C.J.; Plumlee, G.; Ottley, C.J.; Delmelle, P.; Morman, S.; Yazidi, S.E.; Claeys, P.; Kervyn, M.; Elskens, M.; Leermakers, M. Development of a simulated lung fluid leaching method to assess the release of potentially toxic elements from volcanic ash. Chemosphere **2021**, 278, 130303, doi 10.1016/j.chemosphere.2021.130303
4. Malawani, M.N.; Lavigne, F.; Gomez, C.; Mutaqin, B.W.; Hadmoko, D.S. Review of Local and Global Impacts of Volcanic Eruptions and Disaster Management Practices: The Indonesian Example. Geosciences **2021**, 11(3): 109, doi 10.3390/geosciences11030109
5. Carlsen, H.; Valdimarsdóttir, U.; Briem, H.; Dominici, F.; Finnbjornsdottir, R.; Jóhannsson, T.; Aspelund, T.; Gislason, T.; Gudnason, T. Severe volcanic SO_2 exposure and respiratory morbidity in the Icelandic population – a register study. Environ Health **2021**, 20, 23, doi 10.1186/s12940-021-00698-y
6. Nicolaou, L.; Fandiño-Del-Rio, M.; Koehler, K.; Checkley, W. Size distribution and lung-deposited doses of particulate matter from household exposure to biomass smoke. Indoor Air **2021**, 31:51–62, doi 10.1111/ina.12710
7. Dumont, S.; Silveira, G.; Custódio, S.; Lopes, F.; Mouël, J.; Gouhier, M.; Guéhenneux, Y. Response of Fogo volcano (Cape Verde) to lunisolar gravitational forces during the 2014–2015 eruption. Phys Earth Planet Int **2021**, 312, 106659, doi 10.1016/j.pepi.2021.106659
8. Larrue, S.; Paris, R.; Etienne, S. The use of vascular plant densities to estimate the age of undated lava flows in semi-arid areas of Fogo Island (Cape Verde, Atlantic Ocean). J Arid Environ **2020**, 173, 104042, doi 10.1016/j.jaridenv.2019.104042
9. Barrett, R.; Lebas, E.; Ramalho, R.; Klaucke, I.; Kutterolf, S.; Klügel, A.; Lindhorst, K.; Gross, F.; Krastel, S. Revisiting the tsunamigenic volcanic flank collapse of Fogo Island in the Cape Verdes, offshore West Africa. Geol Soc London **2020**, 500, 13-26, doi 10.1144/SP500-2019-187
10. Silva, S.; Alfama, V.; Cardoso, N. The Volcanic Eruption of 2014/15 on Fogo Island Cape Vert and the main effects. Repocs **2016**, v.13, n.26, 49-61. (in Portuguese)
11. Fomba, K.; Müller, K.; van Pinxteren, D.; Poulain, L.; van Pinxteren, M.; Herrmann, H. Long-term chemical characterization of tropical and marine aerosols at the Cape Verde Atmospheric

Observatory (CVAO) from 2007 to 2011. Atmos Chem Phys **2014**, 14:8883–8904, doi 10.5194/acp-14-8883-2014
12. Gama, C.; Tchepel, O.; Baldasano, J.; Basart, S.; Ferreira, J.; Pio, C.; Cardoso, J.; Borrego, C. Seasonal patterns of Saharan dust over Cape Verde - a combined approach using observations and modelling. Tellus B **2015**, 67:24410, doi 10.3402/tellusb.v67.24410
13. Pio, C.A.; Cardoso, J.G.; Cerqueira, M.A.; Calvo, A.; Nunes. T.V.; Alves, C.A.; Custódio, D.; Almeida, S.M.; Almeida-Silva, M. Seasonal variability of aerosol concentration and size distribution in Cape Verde using a continuous aerosol optical spectrometer. Front Environ Sci **2014**, 2:15, doi 10.3389/fenvs.2014.00015
14. WHO. Air quality guidelines for particulate matter, ozone, nitrogen dioxide and sulfur dioxide - Global update 2005, Summary of risk assessment. World Health Organization, **2006**, Geneva, Switzerland
15. Wu, G.; Zhang, X.; Zhang, C.; Xu, T. Mineralogical and morphological properties of individual dust particles in ice cores from the Tibetan Plateau. J Glaciol **2016**, doi 10.1017/jog.2016.8
16. Menut, L.; Bessagnet, B.; Khvorostyanov, D.; Beekmann, M.; Blond, N.; Colette, A.; Coll, I.; Curci, G.; Foret, G.; Hodzic, A.; Mailler, S.; Meleux, F.; Monge, J.-L., Pison, I.; Siour, G.; Turquety, S.; Valari, M.; Vautard, R.; Vivanco, M.G. CHIMERE 2013: a model for regional atmospheric composition modelling, Geosci Model Dev **2013**, 6, 981-1028, doi 10.5194/gmd-6-981-2013
17. Schmechtig, C.; Marticorena, B.; Chatenet, B.; Bergametti, G.; Rajot, J.L.; Coman, A. Simulation of the mineral dust content over Western Africa from the event to the annual scale with the CHIMERE-DUST model. Atmos Chem Phys **2011**, 11:7185–7207, doi 10.5194/acp-11-7185-2011.
18. Ginoux, P.; Chin, M.; Tegen, I.; Prospero, J.; Holben, B.; Dubovik, O.; Lin, S-J. Sources and distributions of dust aerosols simulated with the GOCART model. J Geophys Res **2001**, 106:20255–20274, doi 10.1029/2000JD000053
19. Nishida, H.; Miyai, M.; Tada, F.; Suzuki, S. Computation of the index of pollution caused by heavy metals in river sediment. Environ Pollut **1982**, 4, 4, 241-248, doi 10.1016/0143-148X(82)90010-6
20. Jose, J.; Srimuruganandam, B. Investigation of road dust characteristics and its associated health risks from an urban environment. Environ Geochem Health 2020, 42:2819–2840, doi 10.1007/s10653-020-00521-6
21. Hakanson, L. Ecological risk index for aquatic pollution control, a sedimentological approach. Water Res 1980, 14, 975–1001, doi 10.1016/0043-1354(80)90143-8
22. Aguilera, A.; Bautista, F.; Gutiérrez-Ruiz, M.; Ceniceros-Gómez, A.; Cejudo, R.; Goguitchaichvili, A. Heavy metal pollution of street dust in the largest city of Mexico, sources and health risk assessment. Environ Monit Assess 2021, 193, 193, doi 10.1007/s10661-021-08993-4
23. Ugwu, K.E.; Ofomatah, A.C. Concentration and risk assessment of toxic metals in indoor dust in selected schools in Southeast, Nigeria. SN Appl Sci 2021, 3, 43, doi 10.1007/s42452-020-04099-7
24. Bowen, H.J.M. Trace Elements in Biochemistry; Academic Press: London, UK, 1966
25. RAIS. The Risk Assessment Information System (RAIS); U.S. Department of Energy's Oak Ridge Operations Office (ORO): Oak Ridge, TN, USA. https://rais.ornl.gov/, accessed Apr **2021**
26. Grimsrud, D.T. Project Summary Report to the Legislative Commission on Minnesota Resources (LCMR) Part III: Literature Review of IAQ Impacts on School Children. Continuous Indoor Quality (IAQ) Monitoring in Minnesota Schools. Project Results #2D, **2004**
27. Varshney, C.K.; Padhy, P.H. Total volatile organic compounds in the urban environment of Delhi. J Air Waste Manage Ass **1998**, 48:448-445, doi 10.1080/10473289.1998.10463693
28. Fujita, E.; Campbell, D.; Zielinska, B.; Arnott, W.; Chow, J. Concentrations of Air Toxics in Motor Vehicle–Dominated Environments. Research Report **2011**, 156, Health Effects Institute, Boston, Massachusetts
29. Tassi, F.; Capaccioni, B.; Capecchiacci, F.; Vaselli, O. Non–methane Volatile Organic Compounds (VOCs) at El Chichón volcano (Chiapas, México): Geochemical features, origin and behavior. Geofis Int **2009**, 48:85–95
30. Tassi, F.; Capecchiacci, F.; Cabassi, J.; Calabrese, S.; Vaselli, O.; Rouwet, D.; Pecoraino, G.; Chiodini, G. Geogenic and atmospheric sources for volatile organic compounds in fumarole emissions from

Mt. Etna and Volcano Island (Sicily, Italy). J Geophys Res **2012**, 117, D17305, doi 10.1029/2012JD017642

31. Briber, B.; Hutyra, L.; Dunn, A.; Raciti, S.; Munger, J. Variations in atmospheric CO_2 mixing ratios across a Boston, MA urban to rural gradient. Land **2013**, 2:304–327, doi 10.3390/land2030304
32. Widory, D.; Javoy, M. The carbon isotope composition of atmospheric CO_2 in Paris. Earth Planet Sci Lett **2003**, 215, 289-298
33. Andersson, S.M.; Martinsson, B.G.; Friberg, J.; Brenninkmeijer, C.; Rauthe-Schöch, A.; Hermann, M.; van Velthoven, P.; Zahn, A. Composition and evolution of volcanic aerosol from eruptions of Kasatochi, Sarychev and Eyjafjallajökull in 2008–2010 based on CARIBIC observations. Atmos Chem Phys **2013**, 13:1781–1796, doi 10.5194/acp-13-1781-2013
34. Langmann, B. Volcanic ash versus mineral dust: Atmospheric processing and environmental and climate impacts. ISRN Atmos Sci **2013**, ID 245076, pp 17, doi 10.1155/2013/245076
35. Le Maitre, R.; Dudek, P.; Keller, A.; Lameyre, J.; Le Bas, J.; Sabine, M.; Schmid, P.; Sorensen, R.; Streckeisen, H.; Woolley, A.; Zanettin, A. A classification of igneous rocks and glossary of terms: Recommendations of the International Union of Geological Sciences, Subcommission on the Systematics of Igneous Rocks (No. 552.3 CLA). International Union of Geological Sciences, 1989
36. Escrig, S.; Doucelance, R.; Moreira, M.; Allegre, C. Os isotope systematics in Fogo Island: Evidence for lower continental crust fragments under the Cape Verde Southern Islands. Chem Geol **2005**, 219:93– 113, doi 10.1016/j.chemgeo.2005.02.011
37. Linares, C.; Culqui, D.; Belda, F.; López-Bueno, J.; Luna, Y.; Sánchez-Martínez, G.; Hervella, B.; Diaz, J. Do Saharan Dust Intrusions Affect the Incidence and Severity of COVID-19 in Spain? Environ Sci Pollut Res **2021**, doi 10.21203/rs.3.rs-180563/v1
38. Li, Y.; Padoan, E.; Ajmone-Marsan, F. Soil particle size fraction and potentially toxic elements bioaccessibility: A review. Ecotoxicol Environ Saf **2021**, 209, 111806, doi 10.1016/j.ecoenv.2020.111806
39. Butwin, M.; Pfeffer, M.; Von Lowis, S.; Støren, E.; Bali, E.; Thorsteinsson, T. Properties of dust source material and volcanic ash in Iceland. Sedimentology **2020**, 67, 3067–3087, doi 10.1111/sed.12734
40. Keesari, T.; Pant, D.; Roy, A.; Sinha, U.; Jaryal, A.; Singh, M.; Jain, S. Fluoride geochemistry and exposure risk through groundwater sources in Northeastern parts of Rajasthan, India. Arch Environ Contam Toxicol **2021**, 80, 294–307, doi 10.1007/s00244-020-00794
41. Lavalle-Carrasco, J-; Molina-Frechero, N.; Nevárez-Rascón, M.; Sánchez-Pérez, L.; Hamdan-Partida, A.; González-González, R.; Cassi, D.; Isiordia-Espinoza, M.; Bologna-Molina, R. Recent biomarkers for monitoring the systemic fluoride levels in exposed populations: A systematic review. Int J Environ Res Public Health **2021**, 18, 1: 317, doi 10.3390/ijerph18010317
42. Falcone, E.; Federico, C.; Bellomo, S.; Brusca, L.; D'Alessandro, W.; Longo, M.; Calabrese, S. Impact of acidic volcanic emissions on ash leaching and on the bioavailability and mobility of trace metals in soils of Mt. Etna. Ital J Geosci **2021**, 140 (1): 57–78, doi 10.3301/IJG.2020.22
43. Kabir, H.; Gupta, A.; Tripathy, S. Fluoride and human health: Systematic appraisal of sources, exposures, metabolism, and toxicity, Crit Rev Environ Sci Technol **2020**, 50:11, 1116-1193, doi 10.1080/10643389.2019.1647028
44. Johnston, N.; Strobel, S. Principles of fluoride toxicity and the cellular response: a review. Arch Toxicol **2020**, 94, 1051–1069, doi 10.1007/s00204-020-02687-5
45. Zheng, J.; Noller, B.; Huynh, T.; Ng, J.; Taga, R.; Diacomanolis, V.; Harris, H. How the population in Mount Isa is living with lead exposure from mining activities. Extract Ind Soc **2021**, 8(1), 123-134, doi 10.1016/j.exis.2020.11.008